Supporting Information for Continuum Theory of Electrostatic Correlations at Charged Surfaces

J. Pedro de Souza[†] and Martin Z. Bazant[*,†,‡]

†Department of Chemical Engineering, Massachusetts Institute of Technology, 25 Ames St, Cambridge, Massachusetts 02142 USA

‡Department of Mathematics, Massachusetts Institute of Technology, 182 Memorial Drive, Cambridge, Massachusetts 02142 USA

E-mail: bazant@mit.edu

Phone: 617-324-2036

Derivation of Maxwell Stress

Starting from the equation

$$\nabla \cdot \tau_e = \rho \mathbf{E} = \nabla \cdot (\hat{\varepsilon}\mathbf{E})\mathbf{E}, \tag{S1}$$

the derivation of the Maxwell stress makes use of two vector identities:

$$\begin{aligned} \nabla(\mathbf{A}\cdot\mathbf{B}) &= \mathbf{A}\cdot\nabla\mathbf{B} + \mathbf{B}\cdot\nabla\mathbf{A} \\ \nabla\cdot(\mathbf{A}\mathbf{B}) &= (\nabla\cdot\mathbf{A})\mathbf{B} + \mathbf{A}\cdot\nabla\mathbf{B}, \end{aligned} \tag{S2}$$

for two vectors $\mathbf{A}$ and $\mathbf{B}$, valid when $\nabla \times \mathbf{A} = 0$ and $\nabla \times \mathbf{B} = 0$. Using the permittivity operator $\hat{\varepsilon} = \varepsilon(1 - {\ell_c}^2\nabla^2)$, the expression can be split into two terms that can be analyzed separately,

$$\nabla \cdot \tau_e = \nabla \cdot (\varepsilon\mathbf{E})\mathbf{E} - \nabla \cdot (\varepsilon {\ell_c}^2 \nabla^2 \mathbf{E})\mathbf{E}. \tag{S3}$$

With the requirement of $\nabla \times \mathbf{E} = 0$, the first term can be written as

$$\begin{aligned} \nabla\cdot(\varepsilon\mathbf{E})\mathbf{E} =& \nabla\cdot(\varepsilon\mathbf{E})\mathbf{E} + \frac{1}{2}\varepsilon\mathbf{E}\cdot\nabla\mathbf{E} + \frac{1}{2}\mathbf{E}\cdot\nabla(\varepsilon\mathbf{E}) - \frac{1}{2}(\varepsilon\mathbf{E}\cdot\mathbf{E}) \\ =& \nabla\cdot(\varepsilon\mathbf{E})\mathbf{E} + \varepsilon\mathbf{E}\cdot\nabla\mathbf{E} + \frac{1}{2}\mathbf{E}\cdot\mathbf{E}\nabla\varepsilon - \frac{1}{2}(\varepsilon\mathbf{E}\cdot\mathbf{E}) \\ =& \nabla\cdot(\varepsilon\mathbf{E}\mathbf{E} - \frac{1}{2}\varepsilon\mathbf{E}^2\mathbf{I}) + \frac{1}{2}\mathbf{E}\cdot\mathbf{E}\nabla\varepsilon \\ =& \nabla\cdot(\varepsilon\mathbf{E}\mathbf{E} - \frac{1}{2}\varepsilon\mathbf{E}^2\mathbf{I}), \end{aligned} \tag{S4}$$

with constant ε, where $\mathbf{I}$ is the identity tensor. The second term can be similarly expanded:

$$\begin{aligned}
-\nabla\cdot(\varepsilon{\ell_c}^2\nabla^2\mathbf{E})\mathbf{E} &= -\nabla\cdot(\varepsilon{\ell_c}^2\nabla^2\mathbf{E})\mathbf{E} - \varepsilon{\ell_c}^2\nabla^2\mathbf{E}\cdot\nabla\mathbf{E} \\
&\quad - \mathbf{E}\cdot\nabla(\varepsilon{\ell_c}^2\nabla^2\mathbf{E}) + \nabla(\mathbf{E}\cdot\varepsilon{\ell_c}^2\nabla^2\mathbf{E}) \\
&= -\nabla\cdot(\varepsilon{\ell_c}^2\nabla^2\mathbf{E})\mathbf{E} - \varepsilon{\ell_c}^2\nabla^2\mathbf{E}\cdot\nabla\mathbf{E} - \mathbf{E}\cdot\nabla(\varepsilon{\ell_c}^2\nabla^2\mathbf{E}) \\
&\quad + \nabla(\mathbf{E}\cdot\varepsilon{\ell_c}^2\nabla^2\mathbf{E}) + \mathbf{E}\cdot\nabla(\varepsilon{\ell_c}^2\nabla^2\mathbf{E}) + (\nabla\cdot\mathbf{E})\varepsilon{\ell_c}^2\nabla^2\mathbf{E} \\
&\quad - \nabla\cdot(\mathbf{E}\varepsilon{\ell_c}^2\nabla^2\mathbf{E}) \\
&= \nabla\cdot\big[-\varepsilon{\ell_c}^2(\nabla^2\mathbf{E})\mathbf{E} - \varepsilon{\ell_c}^2\mathbf{E}(\nabla^2\mathbf{E}) + \mathbf{E}\cdot(\varepsilon{\ell_c}^2\nabla^2\mathbf{E})\mathbf{I}\big] \\
&\quad + (\nabla\cdot\mathbf{E})\varepsilon{\ell_c}^2\nabla^2\mathbf{E}.
\end{aligned} \tag{S5}$$

At this point, another product rule must be used:

$$a\nabla a = \frac{1}{2}\nabla(a^2), \tag{S6}$$

where a is a scalar. Applying the above identity gives:

$$\begin{aligned}
&-\nabla\cdot(\varepsilon{\ell_c}^2\nabla^2\mathbf{E})\mathbf{E} = \\
&\quad \nabla\cdot\big[-\varepsilon{\ell_c}^2(\nabla^2\mathbf{E})\mathbf{E} - \varepsilon{\ell_c}^2\mathbf{E}(\nabla^2\mathbf{E}) + \mathbf{E}\cdot(\varepsilon{\ell_c}^2\nabla^2\mathbf{E})\mathbf{I}\big] \\
&\quad + \frac{\varepsilon{\ell_c}^2}{2}\nabla\left((\nabla\cdot\mathbf{E})^2\right) \\
&= \nabla\cdot\big[-\varepsilon{\ell_c}^2(\nabla^2\mathbf{E})\mathbf{E} - \varepsilon{\ell_c}^2\mathbf{E}(\nabla^2\mathbf{E}) + \mathbf{E}\cdot(\varepsilon{\ell_c}^2\nabla^2\mathbf{E})\mathbf{I}\big] \\
&+\nabla\cdot\left[\frac{\varepsilon{\ell_c}^2}{2}(\nabla\cdot\mathbf{E})^2\mathbf{I}\right] - \frac{1}{2}(\nabla\cdot\mathbf{E})^2\nabla(\varepsilon{\ell_c}^2) \\
&= \nabla\cdot\big[-\varepsilon{\ell_c}^2(\nabla^2\mathbf{E})\mathbf{E} - \varepsilon{\ell_c}^2\mathbf{E}(\nabla^2\mathbf{E}) + \mathbf{E}\cdot(\varepsilon{\ell_c}^2\nabla^2\mathbf{E})\mathbf{I}\big] \\
&+\nabla\cdot\left[\frac{\varepsilon{\ell_c}^2}{2}(\nabla\cdot\mathbf{E})^2\mathbf{I}\right],
\end{aligned} \tag{S7}$$

with constant ε and ℓ_c. The final expression for the Maxwell stress is therefore:

$$\begin{aligned}\tau_e =& \varepsilon \mathbf{E}\mathbf{E} - \frac{1}{2}\varepsilon \mathbf{E}^2 \mathbf{I} + \varepsilon {\ell_c}^2 \Big[\left(\mathbf{E}\cdot\nabla^2\mathbf{E}\right) \mathbf{I} - \mathbf{E}\left(\nabla^2\mathbf{E}\right) \\ & - \left(\nabla^2\mathbf{E}\right)\mathbf{E} + \frac{1}{2}\left(\nabla\cdot\mathbf{E}\right)^2 \mathbf{I}\Big].\end{aligned} \tag{S8}$$

One-component plasma around a cylinder

Additional results for the one-component plasma around a cylinder are exhibited in Figs. S1 and S2, using the correlation length scaling $\delta_c = \Xi/\xi$ (the correlation hole size in the needle limit[1]). The figures show the occurrence of Manning criticality in MC simulations, which cannot be reproduced by the BSK theory over the finite domain over which the equations are being solved. Even so, the BSK theory can reproduce the transition to the strong coupling limit. While the condensation phenomenon should only occur at infinite dilution, a finite system size must be chosen for the numerical solution of the BSK equation. The parameter $\Delta = \ln(R_{\text{out}}/R_{\text{cyl}})$ is varied between 6.2 and 13 to ensure numerical accuracy of the solutions over the large domain, depending on the value of δ_c.

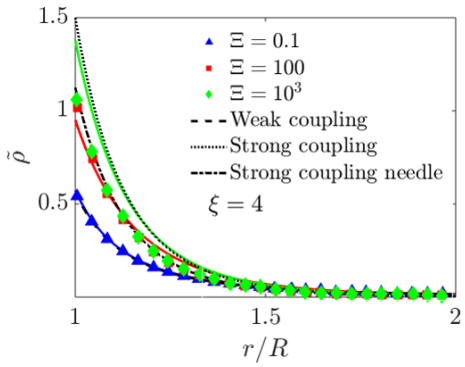

Figure S1: Re-plotted version of Fig. 4 in the main text using a different correlation length scaling. BSK theory compared to additional MC simulations from[1] using $\delta_c = \Xi/\xi$ for the counterion density around a charged cylinder for $\xi = 4$. The labels are identical to Fig. 4 in the main text.

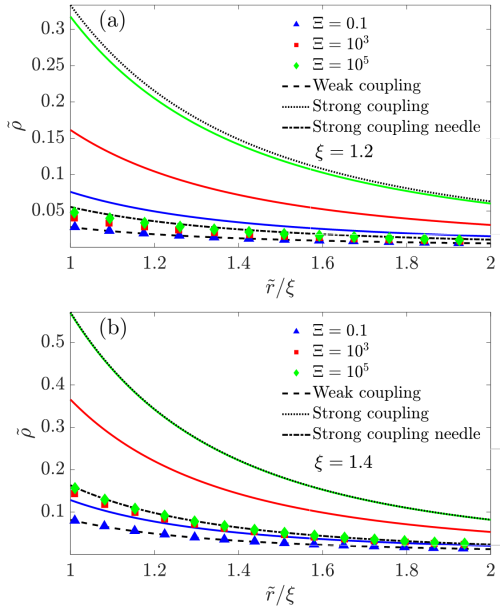

Figure S2: BSK theory compared to additional MC simulations from[1] using $\delta_c = \Xi/\xi$ for the counterion density around a charged cylinder for (a) $\xi = 1.2$ and (b) $\xi = 1.4$. The labels are identical to Fig. 4 in the main text.

Comparison to full electrolyte data set

The comparisons the data from[2] is explored more extensively in Figs. S3, S4, and S5 for $\ell_c = 0.50R_{\text{hole}}$. Respectively, they show the difference of the BSK theory compared to PB theory, the full charge density profiles, and zoomed in profiles into the overscreening region. The BSK theory can closely match the structure of the charge density for many of the plots, including predicting the occurrence of overscreening, with the same correlation length scaling as the one-component plasma. However, at large concentrations, the excess electrochemical potential and ion size effects play a bigger role, leading to inaccuracies of the theory. Even so, the theory is quite adequate up to to provide the correct qualitative corrections up to 1M for the symmetric ions. Note that the MC profiles are shifted by one ion radius, so that the zero x values of the theory and the simulations match. In other words, only the diffuse layer charge density is plotted.

Empirical correlation length scaling in electrolytes

Given the large amount of simulation data on the restricted primitive model, it is possible to leverage the simulation data to fit the correlation length scaling. To define a correlation length that could be used uniformly across many different charge densities, concentrations, and valencies, we used the Grand Canonical MC data from,[2] and fit the correlation length by matching to the charge density profile from an isolated surface with $\varepsilon = 78.5\varepsilon_0$ for a range of conditions: 1:1, 2:1, 3:1, 1:2, and 1:3 ($z_{\text{counterion}} : z_{\text{coion}}$) electrolytes, C_{ref} of 0.01 M, 0.1 M, and 1 M, and q_s of 0.02, 0.04, 0.06, 0.08, 0.1, 0.175, 0.25, 0.375, and 0.5 C/m^2. The finite size of ions with symmetric 0.3 nm diameter is not taken into account in solving the BSK equation. Instead, only the diffuse part of the double layer is plotted, so that the x-axis is shifted by one ionic radius. In some cases, the contact densities for the simulations do not match PB, particularly at higher concentrations and lower charge densities, due to problems with the current assumption of $\mu_i^{\text{ex}} = 0$. In these cases, the profiles cannot be adequately fit by varying the correlation length, and this leads to large errors in the fits. We choose not to add more complexity to the model to capture these exceptional data points, and to rather focus on the electrostatic correlation component. Therefore, we distinguish which fitted values of the correlation length correspond to good fits and which correspond to bad fits. The sum of square error of the fit between the BSK solution and the MC data in units of the PB contact density is chosen as a metric to distinguish between good fits and bad fits. Good fits are defined as those having sum of square error < 0.005.

We can then use the fitted correlation lengths with low error to relate the correlation length to the intrinsic length scales in the system. For example, we can fit the constant α_1 if we assume that the correlation length scales with the $\ell_c = \alpha_1 z^2 l_b$. We can choose α_1 so as to minimize the error between the fitted correlation lengths with low error and the predicted one that is proportional to the Bjerrum length. However, if we fit the correlation length to be proportional to an individual length scale in the system, we see that the fitted correlation length has some dependence on other length scales in the system. For example, we can choose the correlation length scale determined from the one-component plasma, $\ell_c = 0.50R_{\text{hole}}$, and compare it to the fitted correlation lengths

for the electrolyte data set. We find that there is some concentration dependencies, as shown in Figs. S6b and S6e. A more extensive comparison of fitting individual correlation lengths is shown in Fig. S6. One can also observe that the definition of the correlation length based on the Bjerrum length $\ell_c \sim z^2 l_b$ is not the appropriate choice for the correlation length based on the poor agreement between the fitted values and the predicted ones.

Because of the dependence on all length scales, Using only profiles that can be fit with low error, we fit the fitted correlation length, $\delta_{c,\text{fit}}$, to a power law relationship of dimensionless quantities.

$$\delta_c = \alpha_2 \left(\frac{z^2 \ell_B}{\ell_{\text{GC}}}\right)^{\alpha_3} \left(\frac{z^2 \ell_B}{\lambda_D}\right)^{\alpha_4}, \tag{S9}$$

The result is given in Fig. S7 and below:

$$\delta_c = 0.35 \left(\frac{z^2 \ell_B}{\ell_{\text{GC}}}\right)^{-1/8} \left(\frac{z^2 \ell_B}{\lambda_D}\right)^{2/3}, \tag{S10}$$

where z is the counterion valency. This relationship gives the scaling $\ell_c \sim {\ell_B}^{1/4} (q_s/e)^{-1/8} {C_{\text{ref}}}^{-1/6}$. The correlation length scaling is thus a combination of the intrinsic lengths in the system, ℓ_B, $(q_s/e)^{-1/2}$, and ${C_{\text{ref}}}^{-1/3}$. Note that the fitted quantities are represented as fractions so as to emphasize their dependence on the fundamental length scales of the system.

A set of comparisons for the fitted correlation length scaling in Eq. S10 is plotted in Figs. S8 and S9, showing more uniform agreement than the correlation length of $\ell_c = 0.50 R_{\text{hole}}$. Even given the fitted correlation length, it is apparent that for the case where the surface charge density goes to zero, the definition of the correlation length must change. At very low surface charges, the correlation length will be governed by the bulk correlation length of charges. Furthermore, here we only assume a constant correlation length, but it is possible for this length to be dependent on the local concentration or distance from a surface. More studies are necessary to elucidate the spatial dependence of the correlation length, especially when considering multicomponent mixtures with varying ion valency.

References

(1) Mallarino, J. P.; Tellez, G.; Trizac, E. Counterion density profile around charged cylinders: the strong-coupling needle limit. *J. Phys. Chem. B* **2013**, *117*, 12702–12716.

(2) Valiskó, M.; Kristóf, T.; Gillespie, D.; Boda, D. A systematic Monte Carlo simulation study of the primitive model planar electrical double layer over an extended range of concentrations, electrode charges, cation diameters and valences. *AIP Adv.* **2018**, *8*, 025320.

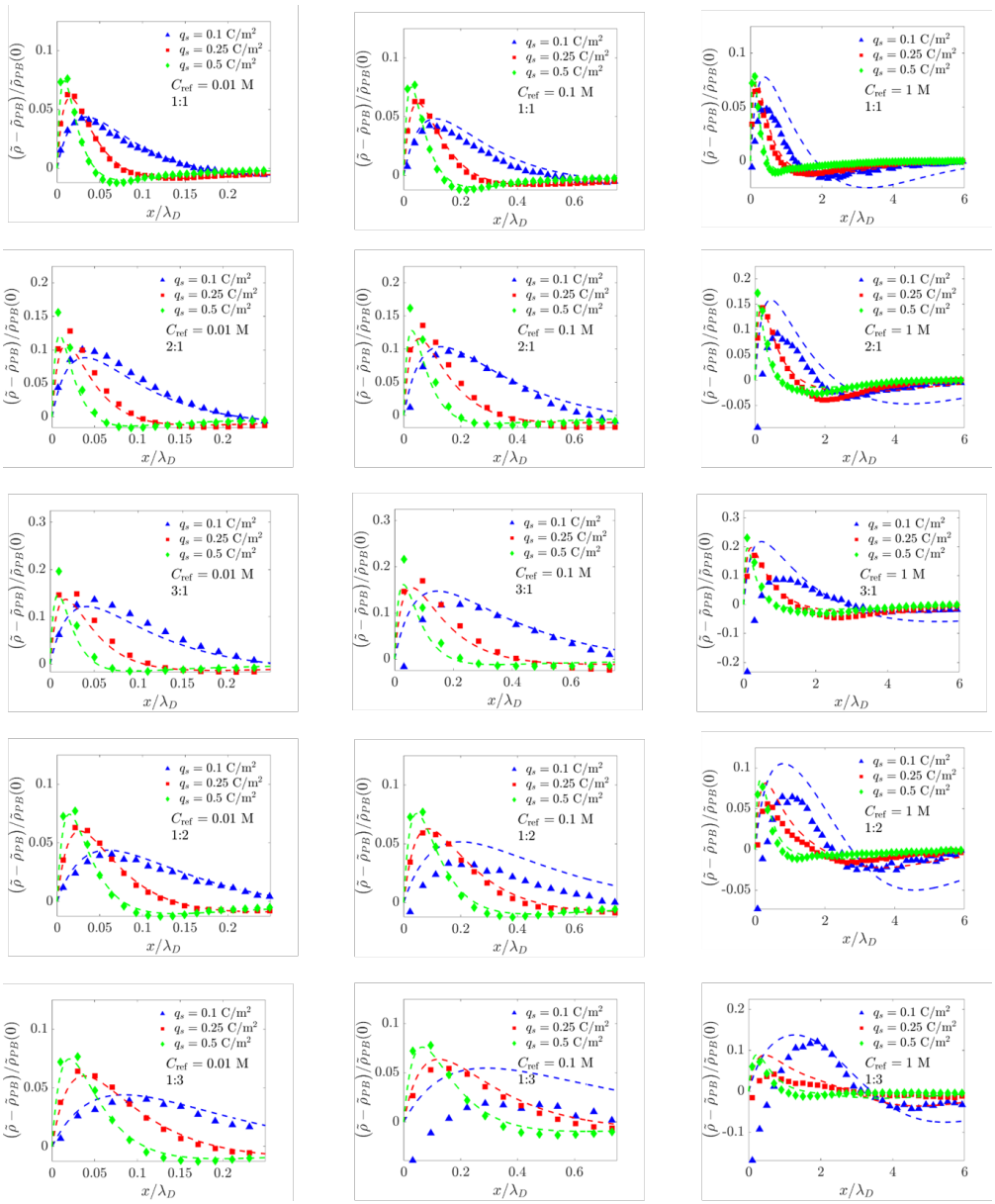

Figure S3: Comprehensive comparison of BSK theory with MC simulations from[2] for the correlation length scaling $\ell_c = 0.50R_{\text{hole}}$ plotted as a difference compared to PB theory. Note that the profiles are organized by $z_{\text{counterion}} : z_{\text{coion}}$ in each row and by C_{ref} in each column.

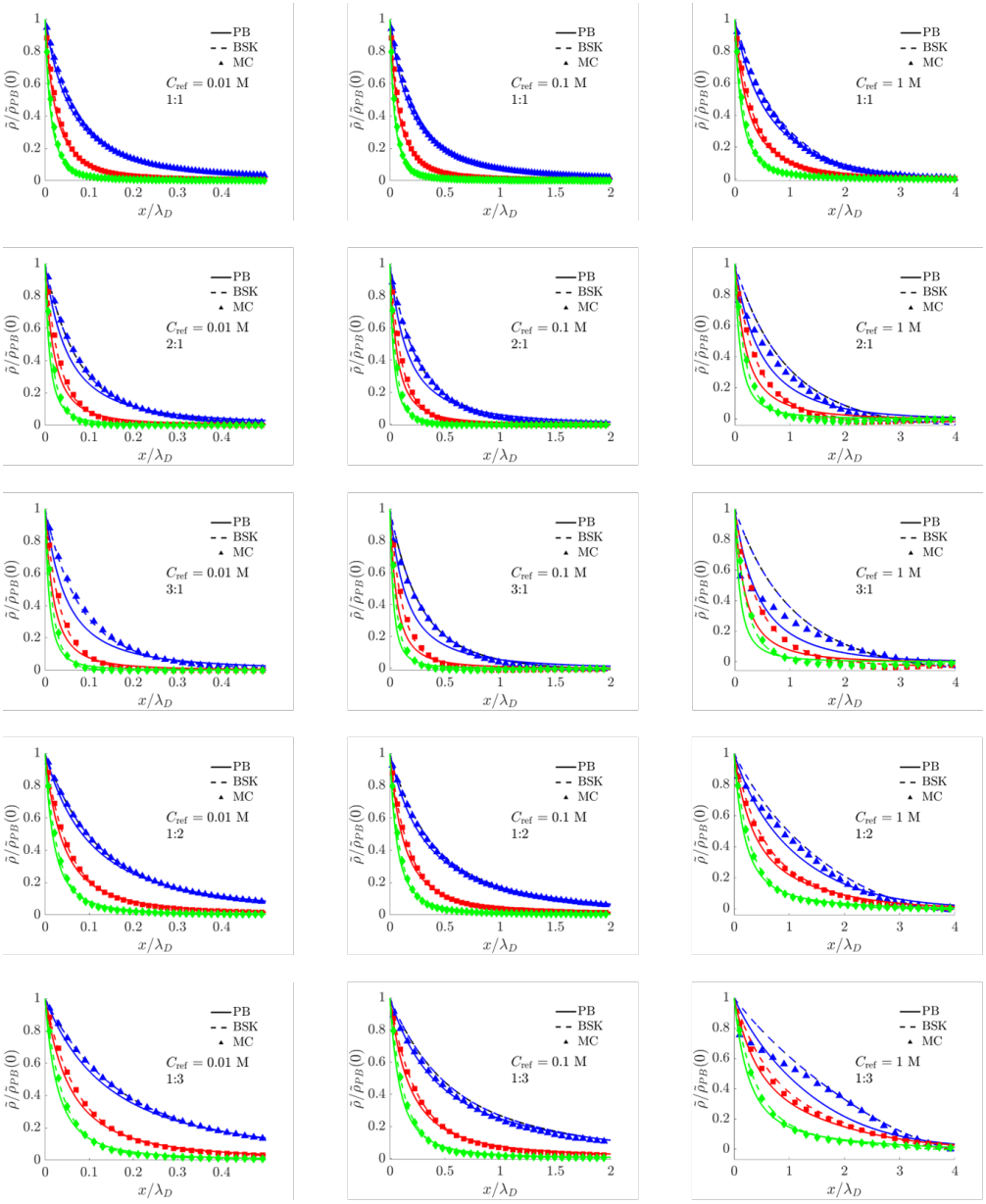

Figure S4: Comprehensive comparison of BSK theory with MC simulations from[2] for the correlation length scaling $\ell_c = 0.50R_{\text{hole}}$ plotted as the total charge density. Note that the profiles are organized by $z_{\text{counterion}} : z_{\text{coion}}$ in each row and by C_{ref} in each column.

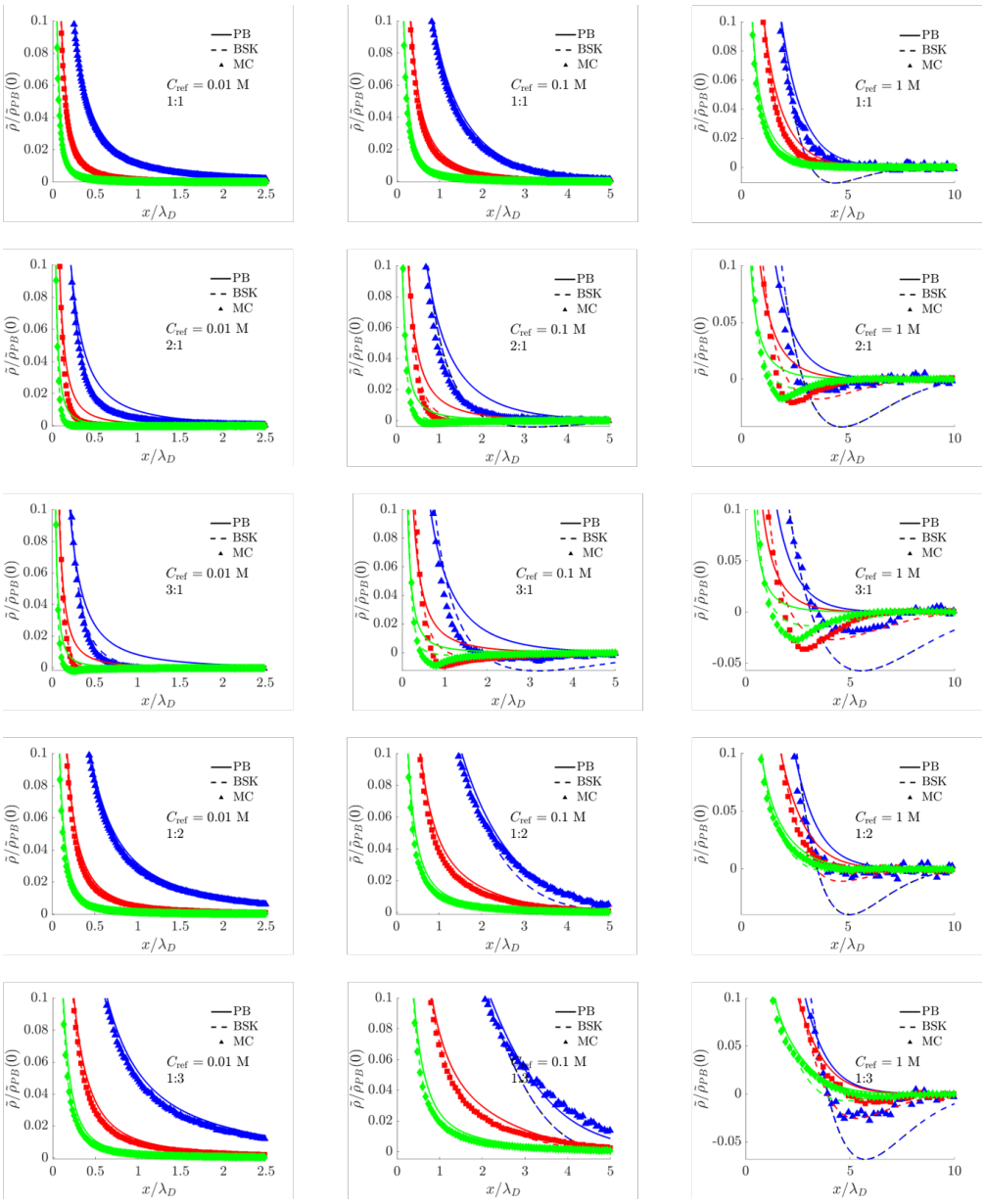

Figure S5: Comprehensive comparison of BSK theory with MC simulations from[2]for the correlation length scaling $\ell_c = 0.50R_{\text{hole}}$ plotted as the total charge density. The axis are zoomed in to isolate the extent of overscreening. Note that the profiles are organized by $z_{\text{counterion}} : z_{\text{coion}}$ in each row and by C_{ref} in each column.

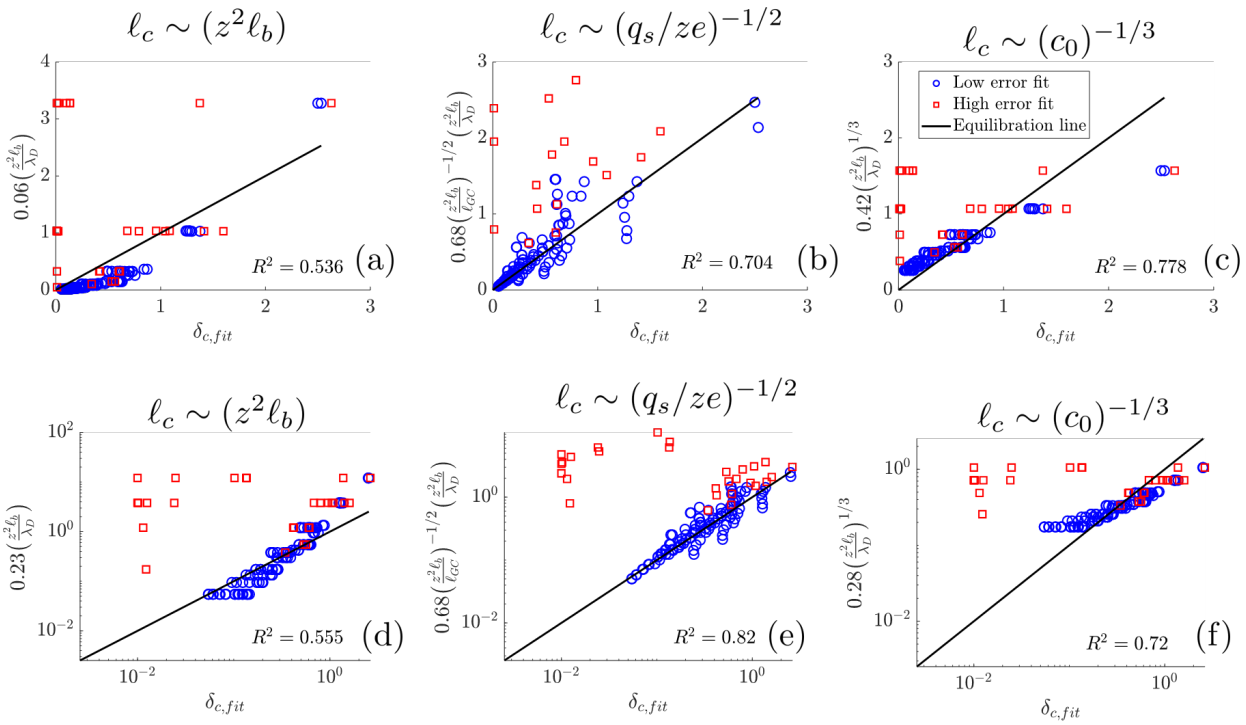

Figure S6: Relating the correlation length to individual length scales in the system. Fitted δ_c values for all simulations are plotted on the x-axis versus the δ_c given by $\delta_c = \ell_c/\lambda_D = \alpha_i \ell_i/\lambda_D$, where $\ell_i = z^2\ell_b$ (a,d), $\ell_i = (q_s/(ze))^{-1/2}$ (b,e), and $\ell_i = c_0^{-1/3}$ (c,f). The top row is plotted on a linear scale, whereas the bottom row is plotted on a log scale. Note that the value of α_i is fit for a, c, d, and f, but is fixed for b and e based on the value determined for the one component plasma ($\ell_c = 0.50 R_{\text{hole}}$).

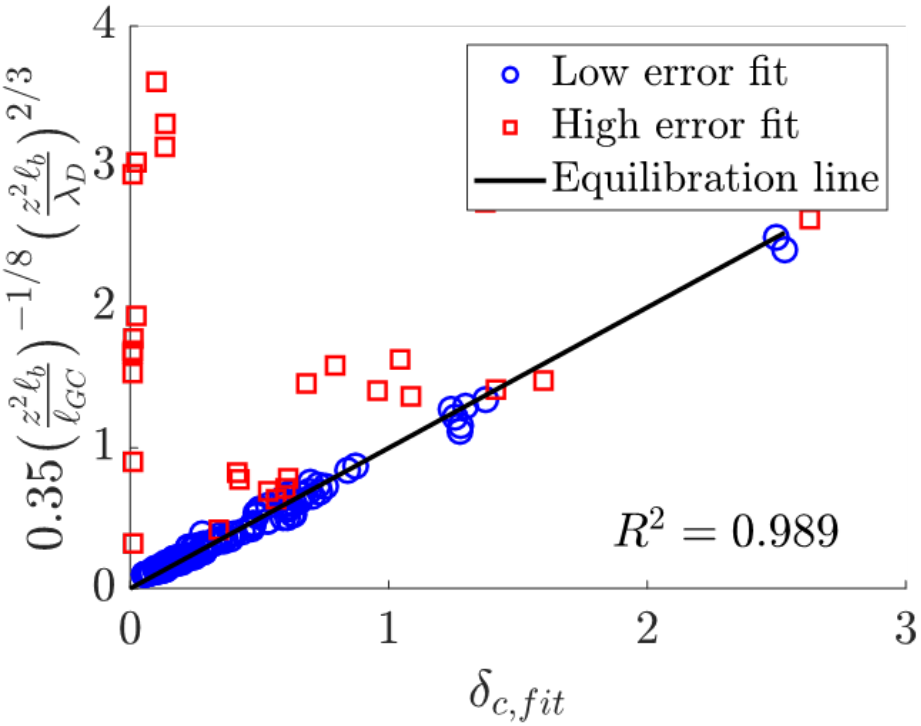

Figure S7: The agreement of the fitted correlation lengths with the scaling from Eq. S10. Fitted δ_c values for all simulations are plotted on the x-axis versus the δ_c given by Eq. S10. The profiles that can be fit with low error are used to determine the fitted scaling (marked in blue).

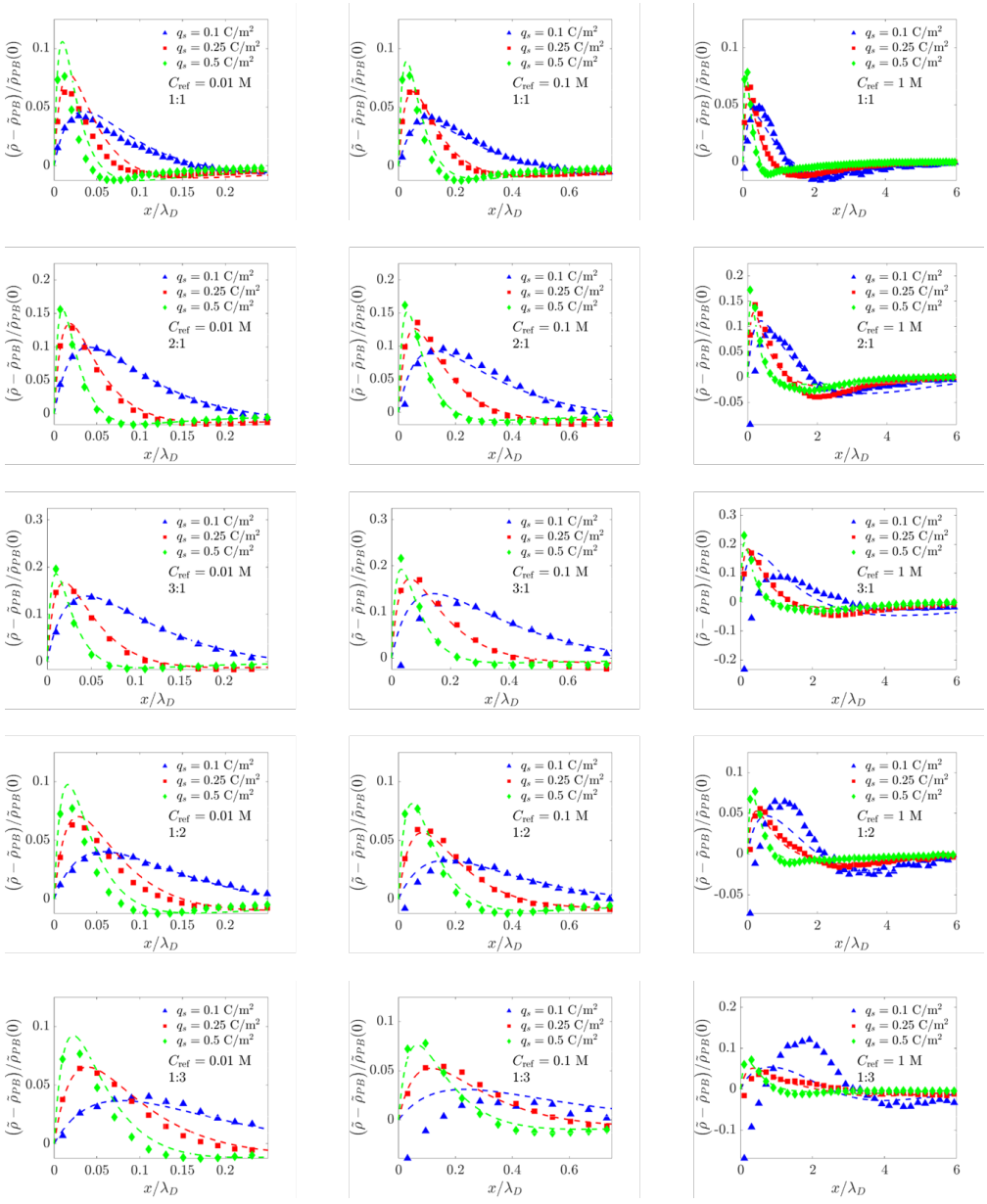

Figure S8: Comprehensive comparison of BSK theory with MC simulations from[2] for the correlation length scaling from Eq. S10 plotted as a difference compared to PB theory. Note that the profiles are organized by $z_{\text{counterion}} : z_{\text{coion}}$ in each row and by C_{ref} in each column.

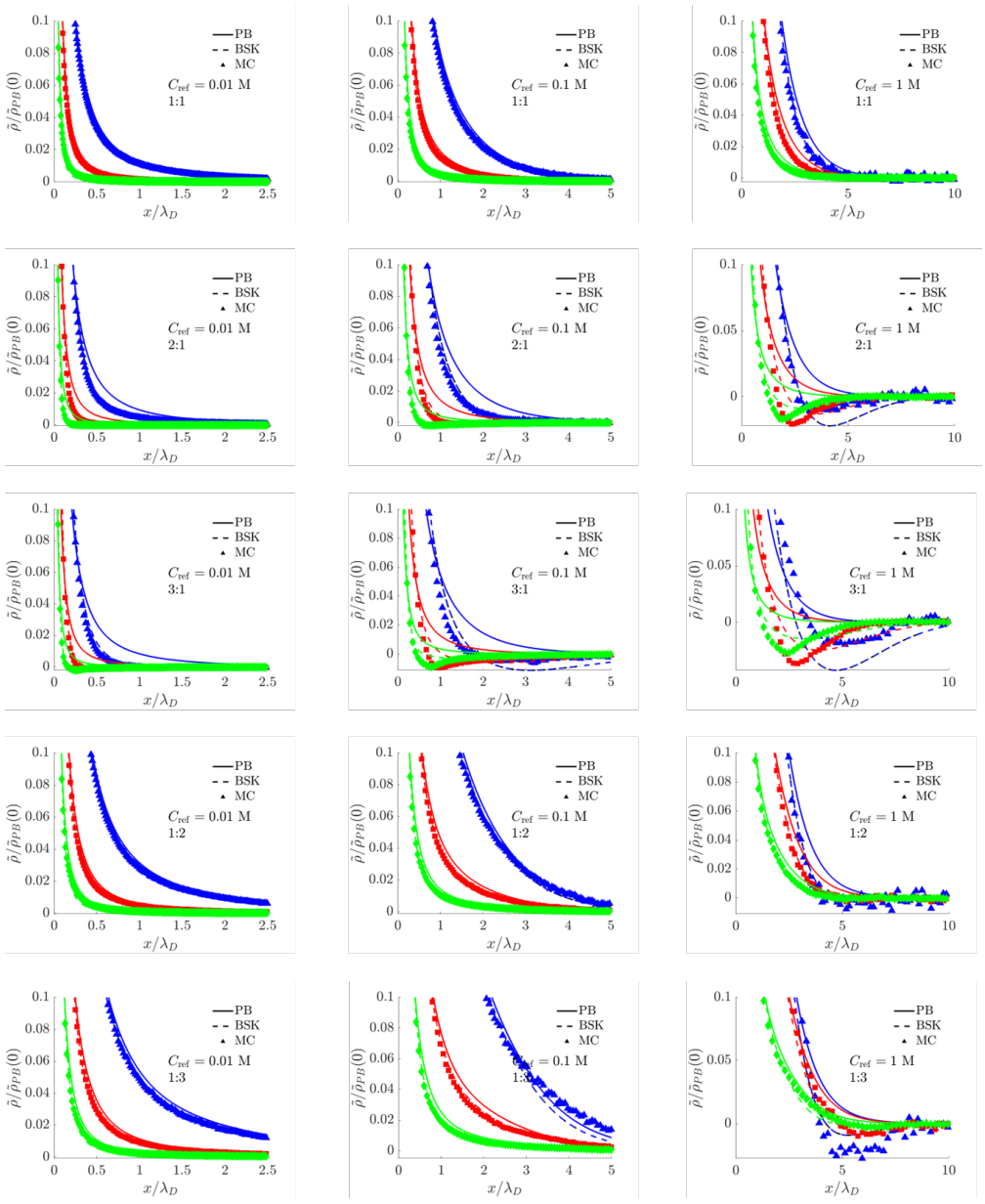

Figure S9: Comprehensive comparison of BSK theory with MC simulations from[2] for the correlation length scaling from Eq. S10 plotted as the total charge density. The axis are zoomed in to isolate the extent of overscreening. Note that the profiles are organized by $z_{\text{counterion}} : z_{\text{coion}}$ in each row and by C_{ref} in each column.